Coherence signatures and density-dependent interaction in a dynamical exciton-polariton condensate

A. Rahimi-Iman,[1,*] A. V. Chernenko,[2] J. Fischer,[1] S. Brodbeck,[1] M. Amthor,[1] C. Schneider,[1] A. Forchel,[1] S. Höfling,[1] S. Reitzenstein,[1,†] and M. Kamp[1]

[1]*Technische Physik, Physikalisches Institut and Wilhelm Conrad Röntgen Research Center for Complex Material Systems, Universität Würzburg, Am Hubland, D-97074 Würzburg, Germany*

[2]*Institute of Solid State Physics, Russian Academy of Sciences, Chernogolovka, 142432 Russia*

(Received 19 May 2012; revised manuscript received 10 August 2012; published 11 October 2012)

We report on pump-power-dependent emission features of a nonthermalized and interacting dynamical condensate of exciton polaritons. The system based on a planar AlAs/AlGaAs microcavity sample with twelve GaAs quantum wells in the active region is investigated comprehensively by measuring the energy-momentum dispersion characteristics, the spatial coherence, and the photon statistics under resonant, fs-pulsed optical excitation at high momentum. We observe a significant polariton-population-dependent modification of the emission signatures above the quantum degeneracy. The nonequilibrium polariton condensate is confirmed by its polaritonic energy-momentum dispersion as well as excitation-power-dependent coherence properties and its photon statistics, being different from that of an ideal coherent state. The polaritonic condensate is characterized by a spatial coherence length of up to 4 μm and a super-Poissonian photon statistic of the emitted light well above threshold. Results obtained in second-order photon autocorrelation measurements in momentum-space resolved spectroscopy indicate polariton repulsive interaction throughout the condensate and a spatial coherence length being shorter than the condensate extension of 20–30 μm.

DOI: 10.1103/PhysRevB.86.155308 PACS number(s): 71.36.+c, 42.65.−k, 73.22.Lp, 42.55.Sa

I. INTRODUCTION

Quantum-well (QW) microcavities (MCs) provide an excellent system for the study of polaritonic condensation effects in solid state. The appearance of strong coupling between QW excitons and light in this semiconductor system leads to the formation of exciton-polaritons.[1] These bosonic quasiparticles can undergo a thermodynamic phase transition towards a macroscopic occupation of the ground state.[2–4] MC polaritons are of particular interest for dynamical Bose-Einstein condensation (BEC) studies because of their light effective mass ($\approx 10^{-4}$–10^{-5} times the excitonic mass), which allows for the observation of condensation features up to room temperature.[5–7] However, using MC-polaritons instead of atomic systems[8,9] results in a nonequilibrium condensation of the Bose particles with a high decay rate. This is why, as long as thermalization is faster than decay, one usually refers to dynamical BECs when condensation occurs in exciton-polariton systems, which nevertheless share many features and signatures such as spatial[3,10,11] and temporal[2,12] coherence that are comparable to a BEC in thermal equilibrium. Polariton BEC, resulting from final state stimulated ground-state occupation of exciton polaritons, has been studied intensively for various exciton-photon detunings in the spectral[13] and time domains[12,14–16] and under the influence of external magnetic fields[17,18] in order to understand features and signatures of the spinor exciton-polariton condensate. It is interesting to note that several schemes for resonant and nonresonant excitation of MC polaritons have been utilized to reach condensation, e.g., nonresonant, continuous wave (cw) excitation in the first absorption maximum,[19] nonresonant ns excitation,[17] excitation into a high-k (k: wave vector) point of the LP branch with ps[2] and ns pulses,[20] and resonant cw excitation at the inflection point.[18] The condensates obtained under various excitation schemes differ from each other in the blue-shift amplitude, critical pump-power densities, distribution of the condensed particles in k space and the thermalization dynamics. These variations occur since condensation is a dynamical process, which is a result of interplay between the increase of the polariton ground-state density and heat dissipation in the system under intensive laser excitation. The degree of thermalization and cooling in the system determines, whether the system is closer to a so called "polariton laser" or to a thermal-equilibrium Bose-Einstein condensate.[21]

In this work, we comprehensively characterize the power-dependent transition of exciton polaritons to a dynamical condensate with respect to its spectral features, its spatial coherence and its photon statistics. In contrast to previous reports using ps excitation, we apply optical fs-pulse excitation into a high-k point of the LP branch much shorter than the average particle lifetime ($\approx$19 ps in the ground state), which is advantageous with respect to the observation of self-interaction features in the system within the particle-reservoir lifetime, and suppresses further perturbations or additional particle injection by the pump laser. This pumping scheme can lead to enhanced population of $k = 0$ polaritons after multistep phonon-assisted cooling into a region around the LP inflection point, where polaritons participate in stimulated scattering into the ground state.[2] The results presented below demonstrate that this fs-excitation scheme is very beneficial to reach a Bose-condensed state.

Our comprehensive study is performed for a condensate system at same experimental conditions, i.e., detuning, temperature, and excitation. Previous studies have focused on various important aspects separately. We measured the condensate in the GaAs system to identify interaction and coherence features of a large spot condensate and to characterize the nonlinearity for polaritonic emission. The following analysis supports the identification of polariton condensation.

First, we present emission characteristics in real-space (near-field: NF) and Fourier-space (far-field: FF) configuration and show a clear polaritonic dispersion above condensation threshold. By a two-spot interference experiment, we show a strong increase of spatial coherence at the nonlinearity, verified by interference patterns in FF spectra, and a spatial coherence length up to 4 μm above threshold. Furthermore, a power-dependent modification of the polariton effective mass above the quantum degeneracy is observed due to a decreased Rabi splitting, which is attributed to high particle densities.[22,23] Eventually, as a signature of interaction, we present a pronounced degree of intensity fluctuations below the level of a thermal emitter and different from that of a coherent state by measuring the second-order autocorrelation function of the condensate emission in the FF configuration.

II. EXPERIMENT

The experiments were performed on a high-Q planar Fabry-Pérot microresonator consisting of a $\lambda/2$-thick AlAs cavity spacer sandwiched between AlAs/$Al_{0.2}Ga_{0.8}As$ distributed Bragg reflectors (DBRs) with 23/27 mirror pairs in the top/bottom DBR. In the central AlAs spacer 4 GaAs QWs, each with a nominal thickness of 13 nm and separated by a 4-nm-thick AlAs layer, were integrated. Two more stacks of four QWs were placed into the first field antinodes of the Bragg mirrors. For the present microcavity, an experimental Q factor of 10 000 was determined,[24] which corresponds to a photon lifetime in the cavity of $\tau_c \approx 7$ ps and an estimated polariton lifetime of 19 ps. The high Q factor of the QW-microcavity sample allows for the study of dynamical polariton condensation at moderate decay rates.

Condensation effects of exciton polaritons in the QW-microcavity sample are studied by pumping polaritons resonantly at an angle of 45 to 50 degrees ($k_{||} \approx 7\ \mu m^{-1}$) with a mode-locked Ti:Sapphire laser. The laser provides pulses with a width of 150 fs at a repetition rate of 82 MHz and a wavelength of 800 nm. We choose to excite the sample via linearly polarized laser light because stimulated ground-state scattering is known to be less efficient under circularly polarized pumping.[19] Resonant pumping provides direct and efficient injection of polaritons at high $k_{||}$ so that the condensate (thus quasiresonantly pumped) is not affected by the external laser induced coherence imprint since incoherent scattering processes such as polariton-polariton and polariton-phonon scattering precede ground-state accumulation.[25] This energy-k-space selectivity in the excitation scheme not only facilitates condensation with spontaneous coherence build-up, but also guarantees strong reduction in the generation of free charge carriers in the QW microcavity system compared to nonresonant excitation, thereby reducing the bleaching of MC polaritons.[22,23] Furthermore, high-energy exciton generation is absent in the formation of exciton polaritons by appropriate resonant pumping. We would like to note that only a small fraction (8%) of the spectrally broadened pump beam ($\sigma_{Gauss} \approx$ 8 meV) is coupled into the system due to spectral selectivity of the highly excitonic polariton mode ($FWHM_X \approx 1$ meV).

The laser light is focused by a 75-mm plano-convex lens onto the sample and side excitation results in an elliptically shaped laser spot with Gaussian intensity distribution of about 40 by 30 μm (FWHM). The rather large dimension of the excitation spot with respect to the diffusion length (a few μm) of the polaritons guarantees a homogenous excitation of polaritons and avoids quantization effects.[27] Eventually, the filtering of resonantly excited photoluminescence (PL) from the sample with cross-polarization techniques and strong suppression of the laser signal by more than six orders of magnitude (the back-scattered laser intensity is much lower than LP emission intensity) enables us to record excitation power-dependent emission patterns of the quasiresonantly pumped condensate.

Time-integrated PL signal is detected by using either NF or FF resolving spectroscopy. In the FF projection, angular resolution of the emission is provided via a microscope objective oriented normal to the sample's surface and two relay lenses. This configuration enables us to probe energy-momentum dispersions in micro-photoluminescence (μPL) experiments directly in two-dimensional (2D) spectra (cf. Ref. 10). From the associated 2D spectrum, cross-sectional line spectra at particular k-space values or regions (k-space integration) can be extracted in a straightforward way for further evaluation. This technique is essential for the detailed analysis of ground-state emission and extracted spectra will further be referred to as $k_{||} = 0$ spectra. PL signal integrated over a certain k-space region will be indicated, e.g., by $k_{||} = (0.0 \pm 0.1)\ \mu m^{-1}$. Moreover, an aperture in the optical path in a real-space projection plane allows for a variable spatial selection (spatial resolution ≈15–20 μm) of the PL signal.

In order to determine the vacuum Rabi splitting as a signature of strong coupling, we first characterize the sample by reflectance measurements using a white light source. Figure 1(a) shows the associated energy dispersion as a function of radial position (radius) on the wafer for the microcavity sample investigated in this work. Here, normalized and inverted $k_{||} = (0.0 \pm 0.1)\ \mu m^{-1}$ reflectivity spectra from a 50-μm-wide spatially selected area are shown in a linear-intensity grey-scale map. From the anticrossing behavior of the lower and upper polariton modes we extract a vacuum Rabi splitting of $E_{Rabi} = 9.5$ meV. For the study of condensation effects, a detuning $\Delta(k_{||} = 0) = E_{C0}\text{-}E_{X0} = 2.83$ meV was chosen, which provides polaritons with an excitonic content, $|X|^2 \approx 64\%$, as marked by an arrow in Fig. 1(a). E_{C0} and E_{X0} represent photon and exciton ground-state energies, respectively.

III. SPATIAL AND MOMENTUM DISTRIBUTION AROUND THE NONLINEARITY

Prior to the discussion of the second-order autocorrelation function, we proceed with the presentation of spectral signatures observed in a comprehensive pump-power-dependent study in order to unambiguously demonstrate dynamical condensation in our polaritonic system. Figure 1 shows a corresponding compilation of Fourier-space (b) and real-space (c) images with linear intensity scale. The images illustrate the evolution of the emission features exemplarily for excitation power densities $P = (1.0, 1.5, 3.5)\ P_{th}$, respectively, where the (time-averaged) threshold power density $P_{th} = 10\ kW/cm^2$

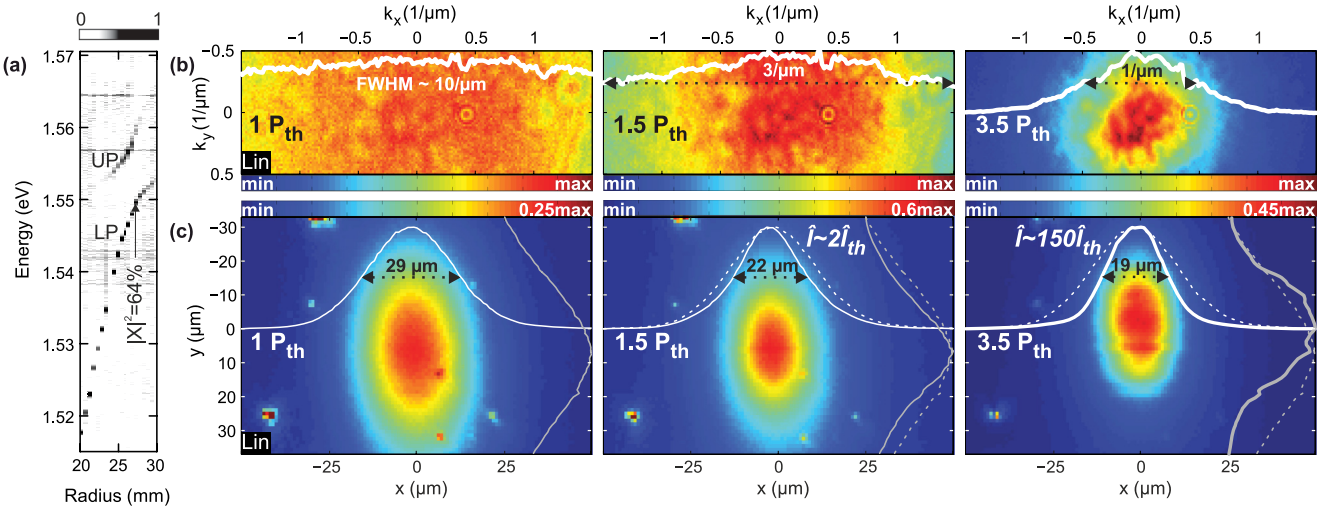

FIG. 1. (Color online) (a) Mapping of the sample reflectivity spectra as function of the radial position with respect to the center of the planar microcavity wafer. The intensity is normalized to the LP resonance absorption and given in arbitrary units. The dispersion of the coupled QW-microcavity system shows a pronounced anticrossing behavior and strong coupling associated with a vacuum Rabi splitting of 9.5 meV. (b) Time-integrated false-color images of the Fourier-space plane are presented for excitation power densities of 1.0, 1.5, and 3.5 times the threshold pump power density P_{th}. A cross-sectional view with normalized intensity is projected (solid white line) for each excitation power density with FWHM values decreasing from 10 to 1 μm^{-1}. (c) In analogy, false-color images of the real-space projection, a microscopy view on the sample surface, are displayed for the same excitation power densities. Again, cross-sectional views, both x and y cut, are projected (solid lines). The dotted line represents the shape at P_{th} for comparison. Shiny spots originate from laser back scattering.

was determined from the input-output characteristics of the system (cf. Fig. 4). Below threshold, a homogenous k-space distribution is observed. A cross-sectional view in the k_x direction with normalized intensity is projected (solid white line) for each power density which reveal a decrease of the FWHM (fitted by a Gaussian curve) from about 10 to 1 μm^{-1} with increasing excitation power.

Images of the real-space projection obtained from a microscopy view of the sample's surface are displayed in Fig. 1(c) for the same pump power densities and normalized cross-sectional views are projected (solid lines). $\hat{I}$ represents the peak intensity of the PL signal. The dotted line represents the shape at P_{th} for comparison. The NF distribution of emission with 30 μm FWHM in the x direction (semiminor axis perpendicular to the side-pump incidence direction) at $P = P_{\text{th}}$ experiences a pronounced spatial narrowing of the high-intensity region above threshold with reduced spatial extension of 19 μm and a modified non-Gaussian profile with steeper flanks at 3.5 P_{th} (cf. cross sections). Within the elliptical pump spot, the emission originates from the condensate and appears to be located closer to the incident side of the excitation beam. The real-space narrowing above threshold results from the Gaussian intensity-distributed beam-shape and the nonlinear responses of the polaritonic system. Essentially, the central, high-intensity part within the pump spot preferentially passes the condensation threshold which explains the real-space narrowing observed in Fig. 1(c). The narrowing in the phase-space distribution seen in Fig. 1(b) clearly indicates the onset of macroscopic ground-state occupation at $k_{||} = 0$, while in real space, the formation of a spatially localized polariton condensate surpassing the lateral extension of the laser spot can be observed (cf. dashed cross-section lines).

IV. SPECTRAL SIGNATURES OF DYNAMICAL POLARITON CONDENSATION

Next, we study the polaritonic character of the condensate by analyzing the mode dispersion of the LP via FF spectroscopy. Compared to a photonic dispersion, which is parabolic in planar microcavities, the LP branch exhibits an inflection point at specific k vectors ($\approx$1–2 μm^{-1}). Thus the polaritonic emission can be identified via energy dispersions extracted from 2D FF spectra. In Fig. 2(a), we show corresponding FF dispersions of polariton modes at a detuning $\Delta = 2.8$ meV, corresponding to an excitonic fraction $|X|^2 \approx 64\%$. The k-space coverage amounts to ± 2.3 μm^{-1} and different excitation densities of 0.05, 1.0, 1.5, 2.0, and 4.2 times the threshold pump density were chosen. Each FF dispersion is normalized to its maximum intensity and split into two linked parts with linear (left) and logarithmic (right) intensity profiles to provide distinguished contrasts in the false-color diagram. The profiles are rendered with lighting for the sake of an improved visualization of the dimensionality and proportions of the emission mode. The projected lines show the corresponding LP dispersion (dashed, white), a virtual cavity mode (C^*, dotted, green) aligned to the ground state $k_{||} = 0$ and the maximum intensities for each k vector (black dots), while the bare exciton ($E_{X0} = 1.5511$ eV) and photon ($E_{C0} = 1.5539$ eV) dispersions are not shown. In between, 2D NF spectra are displayed for pump rates $P/P_{\text{th}} = 1.0$, 1.5, and 2.0, from left to right, respectively, with the same energy scale.

Emission features depicted in Fig. 2(a) for FF and NF configurations show typical trends and features of a nonlinearity in the polaritonic system: a blue shift in energy (0.75 meV) plus spectral, momentum, and spatial narrowings above the condensation threshold. The first trend serves as

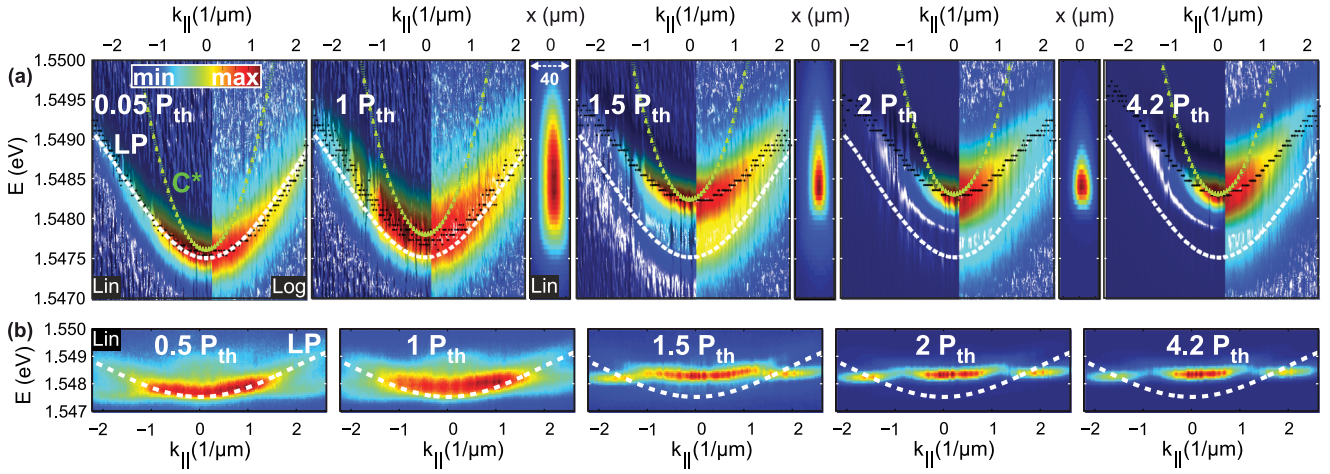

FIG. 2. (Color online) (a) Time-integrated energy-momentum dispersion of polariton modes at a detuning $\Delta = 2.8$ meV ($|X|^2 \approx 64\%$), for different threshold-normalized pump powers. Each Fourier-space spectrum (rendered with lighting) is normalized to its maximum intensity and split into two linked parts with linear (left) and logarithmic (right) intensity profiles. Projected lines show the corresponding polariton dispersion (LP, dashed, white), and a virtual cavity mode (C*, dotted, green) aligned to the ground state. Black dots mark the maximum intensities for each k vector. The pump power increases from left to right. In between, 2D real-space spectra for pump densities $P/P_{\text{th}} = 1.0$, 1.5, and 2.0 are displayed, from left to right, with the same energy scale which show the spatial distribution of emission. (b) Pump-power-dependent first-order spatial coherence represented by interference patterns in the Fourier-space spectrum (a), which is generated by applying a double-slit corresponding to a 3-μm spatial separation in the real-space plane projection. As a guide to the eye, the LP dispersion (dashed, white) is drawn into the linear intensity profile spectra.

an indicator of a high population density in the ground state, while the latter two are signatures for an increase of temporal and spatial coherence. For a detailed analysis and discussion of interaction features and ground-state occupation of the dynamical condensate, we extracted $k = 0$ cross sections as well as momentum space and energetic population distributions, which are described and discussed below.

A. First-order spatial coherence

Another strong indicator of a condensation threshold within the comprehensive study of our high-Q polaritonic system, namely, enhanced spatial coherence, can be accessed by energy and Fourier-space resolved double-slit interference measurements.[10,11] The evolution of corresponding interference patterns in Fourier-space spectra with increasing pump densities is presented in Fig. 2(b) for emission at $P/P_{\text{th}} = 0.5$, 1.0, 1.5, 2.0, 4.2.[29] Similar to Fig. 2(a), the uncondensed LP dispersion (dashed, white) is projected onto the spectra in Fig. 2(b). For these measurements, a spatial spot separation $r = r'/M$ on the sample surface is achieved by inserting a double slit with slit separation r' in the NF projection plane. Here, M denotes the optical magnification in the NF plane. Figure 3(a) presents a schematic drawing of such a projection. In Fig. 3(b), a reference FF interference pattern is shown,[30] measured for the pump laser spot on the sample. The visibility amounts to >90% for $r \approx 6$ μm, reflecting the large coherence length of the laser. For the LP below threshold, no interference fringes are obtained in Fig. 2(b). However, at pump densities above threshold, fringes occur at $|k| \approx 1.5$ μm^{-1} and line-up with the partially coherent energy state with a characteristic k-space separation corresponding to the spatial separation r which amounts to $\approx$3 μm. This separation is on the order of the system's coherence length above threshold [cf. Fig. 3(d)], thus revealing a pronounced increase of the visibility with increasing pump-power. Please note that although the interference lobes overlap with the dispersion around 1.5 μm^{-1}, the signal does not depend on the dispersion in the first place and in the corresponding spectrum in Fig. 2(a), no emission is seen from k ≈ 1.5 μm^{-1} at $P > P_{\text{th}}$. For a given pump rate, one can vary the slit separation and observe a specific change in the k-space location of the lobes,[10] clearly distinguishing it from higher-k polaritonic emission. The obtained intensity modulation is described by a term proportional $|g^{(1)}(r = |r_1 - r_2|)| \cos(2r\, k_{||})$, where r_1 and r_2 denote the location of the separated spots on the sample. The degree of spatial coherence $|g^{(1)}(r)| = V$ is given by the visibility V of the interference pattern and reaches up to 60% at 4 P_{th}. In Fig. 3(c), k-space ground-state cross sections of the FF double slit spectra with normalized intensities $[I/\hat{I}(E_0), E_0$: LP ground-state energy] are shown from which visibilities are extracted.

Before addressing the power-dependent trend of V, we focus on the spatial coherence length d_c of our condensed polaritons. Figure 3(d) shows the decrease of $g^{(1)}(r)$ with increasing separation r for two pump rates above threshold of the polariton condensate. We derive d_c at $g^{(1)}(r) = 1/\text{e}$ for respective pump rates. For 1.7 P_{th}, $d_c \approx (3.0 \pm 0.2)$ μm, while for 3.5 P_{th}, $d_c \approx (4.0 \pm 0.3)$ μm. The increase of $g^{(1)}(r)$ and d_c as a consequence of stronger pumping is good proof of spontaneous coherence build-up in a partly thermalized large-spot condensate above the threshold [cf. Fig. 2(b)]. However, the short lifetime of the pulsed condensate only provides a short interaction time that does not allow for the formation of extended spatial coherence.

B. Macroscopic ground-state population

Focusing on the ground-state occupation, Fig. 4 summarizes the analysis of $k = (0 \pm 0.2)$ μm^{-1} line spectra extracted

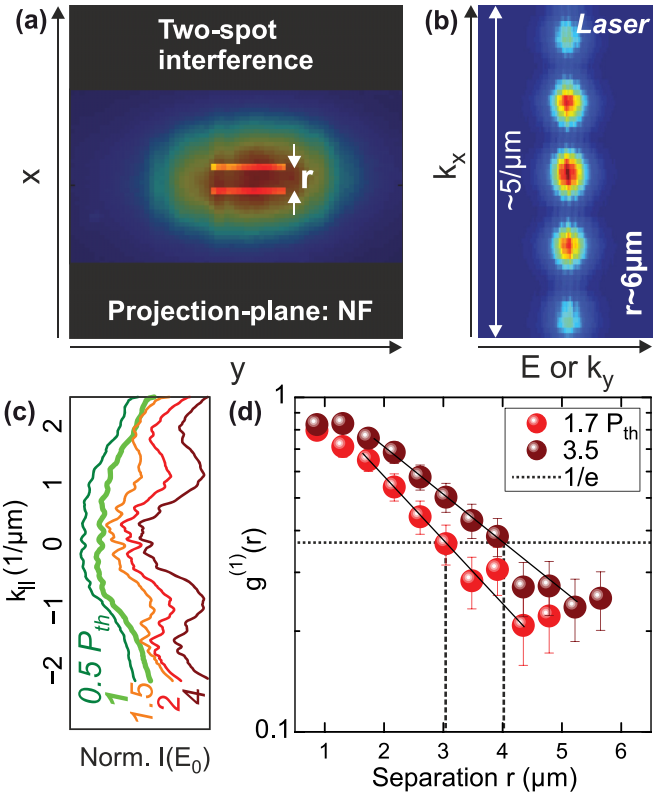

FIG. 3. (Color online) (a) Scheme of two-spot interference indicating the slit separation in real space. (b) Representative fringes acquired from back-scattered light from the pump laser spot in the phase space (k_x vs k_y) or E-k diagram (k_x vs E) with interference fringe visibility >90%. (c) k-space-oriented ground-state cross sections of the FF double slit spectra shown in Fig. 2(b). (d) First-order spatial coherence $g^{(1)}(r)$ of a polariton condensate at 1.7 and 3.5 $P_{\rm th}$. With increasing spatial separation r of emitters the measured values surpass 1/e (dotted line) at 3 and 4 μm (vertical dashed lines), respectively, which represent the spatial coherence length d_c at the given pump densities. Solid lines indicate the exponential decay as guides for the eye.

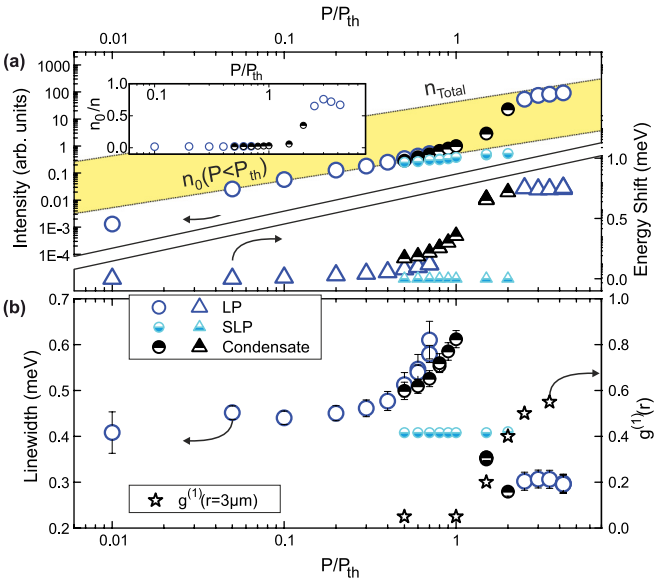

FIG. 4. (Color online) (a) Input-output diagram showing the pump-power-dependent nonlinear increase of time-integrated emission from the LP ground state $k = (0 \pm 0.2)\ \mu\text{m}^{-1}$. Blue open circles represent the (integrated) intensities below and above threshold, normalized to the threshold value. Close to threshold individual double-mode fitting of the LP signal was necessary to match the data acquired from the pulsed signal with time integration. Data from the stronger mode associated with emission from the condensate (black) and from the uncondensed LP mode (light blue) are plotted with half-filled circles. The relative energy shift of these modes is plotted in the same diagram with triangles. (Inset) Condensate fraction n_0/n vs $P/P_{\rm th}$. (b) Linewidth of the power-dependent polariton signal as a measure of first-order temporal coherence. In addition, the first-order spatial coherence $g^{(1)}(r)$ measured with the double slit corresponding to a 3-μm spatial separation [cf. Fig. 2(b)] is plotted in the same graph (stars, right scale).

from 2D images. The figure shows important features of a quantum degeneracy threshold that gives rise to coherent emission of radiation above threshold pump power. From a Lorentzian lineshape fitting of the LP ground-state signal, we obtain the characteristic s-shaped input-output curve with a nonlinear increase of emission above threshold as shown in Fig. 4(a). Blue circles represent the integrated intensities below and above threshold, normalized to the threshold value. In the threshold region, double-mode fitting of the LP signal was necessary to describe the time-integrated PL data under pulsed excitation [cf. Fig. 2(a)]. Here, we assume that during the temporal evolution of the pulse, the weakly occupied "simple" LP (SLP) branch remains at the low pump energy and exhibits no spectral broadening, while the condensed polaritons experience an energy blue shift and a change in the linewidth. The emerging stronger condensate mode at higher energy (black) and the SLP mode (light blue) are plotted with half-filled symbols.

An estimation of the total polariton population based on life-time considerations and the emission intensity distribution in momentum space (discussed later in this section) is represented in Fig. 4(a) by the line labeled $n = n_{\rm Total}$. Below threshold, the population of the ground state shows a *linear* increase [line labeled $n_0(P < P_{\rm th})$]. In this diagram, a clear rise in the output by two orders of magnitude is seen above the threshold. The fractional population n_0/n as a function of $P/P_{\rm th}$ is shown in the inset, where a condensate fraction of more than 0.5 is obtained above the threshold (cf. Ref. 28). Further above threshold, this fraction decreases due to saturation effects caused by local heating in the sample at strong pump rates.

In Fig. 4(a), right scale, a gradual increase of the mode energy with increasing pump densities is presented. Above threshold, an energy shift of up to 0.75 meV is measured, a value 4 meV lower than E_{X0} and 7.75 meV lower than E_{C0} providing additional evidence for a polaritonic condensate. The more polaritonic quasiparticles are in the system, the stronger are the repulsive interaction and the resulting blue shift of the condensate energy, as discussed in the literature for polariton condensates[28,31] with repulsive fermionic exchange interaction between QW excitons of the same spin[32,33] and a

reduced normal-mode splitting due to phase-space filling.[34] However, local heating of the excitation spot also needs to be taken into account, as discussed later when presenting above threshold dispersions.

The power-dependent emission linewidth, which is plotted in Fig. 4(b) with symbols corresponding to Fig. 4(a), serves as a measure of first-order temporal coherence. A clear broadening of the LP emission takes place close to threshold until a significant drop occurs, indicating a build-up of coherence in the ground state. This is also in line with the first-order spatial coherence function $g^{(1)}(r)$ analyzed in Fig. 2(b) and plotted in the same graph of Fig. 4(b) (stars, right scale). The significant enhancement of the interference pattern clearly correlates with the threshold. This agrees well with previous results[10,11] and theoretical analysis by Doan *et al.*[35]

It is often argued that individual features of this dynamic and self-interacting exciton-polariton system plotted in Fig. 4 are similar to that of a photon laser.[21] Indeed, only a detailed study including in particular the mode dispersions at respective pump powers as well as population considerations can rule out the occurrence of photonic lasing and the system's transition from strong to weak coupling.

Figure 5(a) shows measured $E(k)$-dispersions at pump powers of (0.05, 0.5, 1.0, 1.5, 2.0, and 4.2) P_{th}, labeled by open symbols. Here, a transition from the uncondensed LP dispersion at low pump to a polariton-condensate-like dispersion above threshold is evidenced. The uncondensed LP dispersion (white, dotted) and a virtual (parabolic) cavity dispersion C* (black, dotted) as well as a fictional broader parabola $\sim k^2$ (gray/light blue, dotted) aligned to the condensate ground-state are drawn on the image. There is neither a congruence between the measured condensate dispersion with C* nor with the broadened parabola (mimicking a dramatic change of the effective index of refraction n_{eff} in the cavity). If assigning measured mode shifts to a change of n_{eff}, the variation of n_{eff} must be on the order of 1%, resulting in little change of the effective photon mass $m_{\text{cav}} = 2\pi\hbar n_{\text{eff}}/c\lambda_0$ and thus the photonic dispersion C* (λ_0: photonic emission wavelength in vacuum). Indeed, above threshold, the energy dispersions depicted in Fig. 5(a) deviate clearly from a parabolic characteristic and reveal inflection points at about 1–2 μm^{-1}, as expected from a polaritonic system.

Figure 5(b) shows an increase of the dispersion slopes $\Delta E/\Delta k$ extracted at $k \approx 1/\mu\text{m}$ with increased pump power. From this, we deduce a power-dependent decrease of the effective particle mass above threshold for polaritons occupying the condensate ground state. On one hand, this is seen as a signature of previously mentioned high-density-related interaction effects and a reduction of the normal-mode splitting.[25] On the other hand, the changes are at the same time caused by local heating and the particle-density-related change of the QWs' index of refraction reducing the cavity mode energy.[26] This is confirmed by LP dispersion fits for $P > P_{\text{th}}$. At 1.5 P_{th}, $E_{X0} = 1.5505$ eV, $E_{C0} = 1.5539$ eV, and $E_{\text{Rabi}} \approx 7.3$ meV (corresponding Δ: 3.3 meV). The exciton energy redshift of -0.6 meV is explained as the superposition of an interaction-caused blueshift and an expected local-heating-dependent redshift. In Fig. 5(c), the energies of the bare exciton (red x) and photon (green star) mode extracted from polaritonic dispersion fits are depicted with respect to P/P_{th}. With increasing pump powers, the fitted exciton mode blue shifts to $E_{X0} = 1.5511$ eV and the fitted photon mode tunes red to 1.5530 eV, causing a detuning change. Only this modification of parameters allowed for a precise matching of theoretical LP curves with the measured dispersions, while the Rabi splitting remained constant at ≈7.3 meV in the range of 1.5 to 4.2 P/P_{th}, taking into account respective (constant) ground-state energies of the condensed mode and effective particle masses at corresponding pump rates.

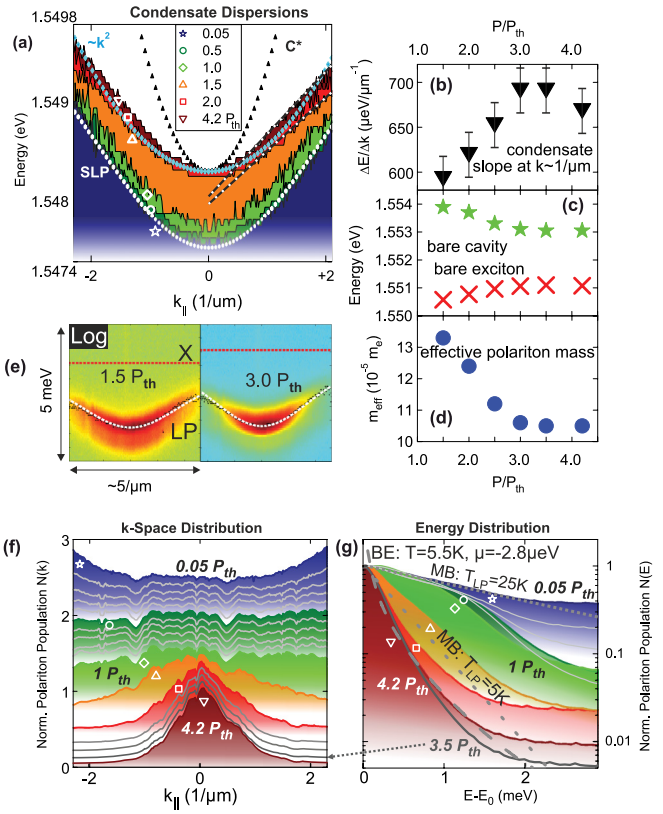

FIG. 5. (Color online) (a) Measured polariton dispersions below and above threshold corresponding to pump powers ranging from 0.05 to 4.2 P_{th}, labeled by white open symbols. The uncondensed LP dispersion (white dotted) and a virtual cavity dispersion (C*, black dotted) as well as a broader parabola ($\sim k^2$, gray/light blue dotted) aligned to the condensate ground-state are drawn into the image. (b) Linear slope $\Delta E/\Delta k$ extracted from the dispersion region at $k = 1\ \mu\text{m}^{-1}$ vs P/P_{th} above threshold. (c) Bare exciton and photon mode energies which allowed for best dispersion fits. (d) Effective polariton mass vs P/P_{th}. (e) Fitted condensate dispersion for respective pump rates 1.5 and 3.0 P_{th} (logarithmic intensity profile). (f) Estimated polariton population $N(k)$ for the modes presented in (a) and (e) normalized to the $k = 0$ value showing a pronounced occupation of the ground state above threshold. (g) In analogy to (f), the estimated polariton population $N(E)$ with respect to the corresponding ground-state energy E_0 is depicted and demonstrates strong spectral narrowing of the population distribution above threshold and a transition from Maxwell-Boltzmann (MB) distribution (dotted gray line with $T_{\text{LP}} = 25$ K) and a Bose-Einstein-like (BE) distribution (dashed gray curve with $T = 5.5$ K and $\mu = -2.8\ \mu$eV, cf. Ref. 36). Populations are each normalized to the ground-state value for clarity.

The experienced reduction of the detuning Δ, which modifies the excitonic fraction of the ground-state LPs, results finally in a decrease of the effective polariton mass m_{eff}, shown in Fig. 5(d). The mass is obtained by fitting an energy parabola with $E = \hbar^2 k^2 / 2 m_{\mathrm{eff}}$ to the modeled LP dispersion at low k vectors $<0.8/\mu$m. For the uncondensed LP dispersion, an effective polariton mass of $(10.8 \pm 1.0) \times 10^{-5}\, m_0$ (electron masses) was determined. By the change of Rabi splitting, an increased $m_{\mathrm{eff}} = (13.3 \pm 1.0) \times 10^{-5}\, m_0$ was extracted at 1.5 P_{th}, which decreased to $(10.5 \pm 1.0) \times 10^{-5}\, m_0$ at 4.2 P_{th} as a result of the detuning change. This trend well mirrors the obtained trend of the dispersion slopes at $k \approx 1\ \mu\mathrm{m}^{-1}$ shown in Fig. 5(b). In Fig. 5(e), we show the measured dispersions with logarithmic intensity profile for 1.5 P_{th} and 3.0 P_{th}.

The momentum-space distribution of polaritons provides important information about the evolution and formation of a condensate and its thermodynamic properties. Such an analysis was summarized by Deng *et al.* and compared to numerical simulations.[31] Here, we briefly show a behavior typical for dynamical condensation obtained from our time-integrated measurements. Figure 5(f) presents the estimated polariton population $N(k)$ for the modes analyzed in Figs. 4 and 5, normalized to the $k = 0$ values. Therefore, for each pump-rate, the spectral intensities $I(k;\ 1.547\ \mathrm{eV} < E < 1.550\ \mathrm{eV})$ (dips are caused by acquisition defects) have been weighted with the estimated lifetimes $1/\tau_{\mathrm{LP}}(k) = |C|^2/\tau_C + |X|^2/\tau_X \approx |C|^2/\tau_C$ according to the particles' excitonic and photonic fractions $1 = |X|^2(k) + |C|^2(k)$ at given k vectors with lifetimes $\tau_X \gg \tau_C = 7$ ps. The estimated distribution of the polaritonic quasiparticles reveals a clear transition from an LP distribution with highly populated reservoir to a macroscopically occupied ground-state with increasing power where ≈68% of the emitters lie within one standard deviation of a normal distribution.

Moreover, as expected for the formation of a dynamical condensation, the transition from a Maxwell-Boltzmann (MB) to a Bose-Einstein-like (BE) distribution takes place with increasing power. The power-dependent energetic polariton distribution $N(E)$ with respect to the ground-state energies E_0 can be probed via k-space-integrated and lifetime-corrected intensities $I(E\text{-}E_0;\ k_{||} = 0 \pm 2.4\,\mu\mathrm{m}^{-1})$. In Fig. 5(g), one can see a strong spectral narrowing of the population distribution above threshold. For clarity, $N(E)$ is normalized to the value at E_0 and plotted in semilogarithmic scale. While well below threshold, an MB curve can be fitted to the distribution of polaritons with a gas temperature of $T_{\mathrm{LP}} = 25$ K (cf. MB distribution with $T_{\mathrm{LP}} = 5\ K$), at high pump-rates above threshold, the distribution rather matches a BE curve with $T = 5.5$ K and chemical potential $\mu = -2.8\ \mu$eV (from Doan *et al.*),[36] and does not match the MB curve at lattice temperature (4–5 K). This can only be explained by enhanced thermalization of the condensed bosonic gas, i.e., the transition to a quasiequilibrium Bose gas.[37] The strongest signature of ground-state occupation is found around 3.5 P_{th}, which is consistent with the trend in Fig. 5(b) and the inset of Fig. 4(a). At 4.2 P_{th}, we observe a slight reduction in the ground-state accumulation. Having demonstrated the formation of a nonequilibrium dynamical condensate, we now focus on the excitation power-dependent photon statistics of emission from the system under investigation.

C. Second-order time correlations of interacting polaritons

Autocorrelation experiments provide a valuable tool to characterize the photon statistics of light sources. For instance, in the case of a transition from thermal emission to the emission of coherent light from a laser, the second-order correlation function's value decreases from 2 to 1 for simultaneously registered photons. The second-order autocorrelation function at zero delay is defined by

$$g^{(2)}(\tau = 0) = \langle : \hat{n}^2 : \rangle / \langle \hat{n} \rangle^2, \tag{1}$$

where $\hat{n}$ denotes the photon number operator and colons the normal ordering of the underlying photon field operators.[14] The experimentally obtained value $G^{(2)}(0)$ represents the time-averaged $g^{(2)}(0)$ over each pulse.[2] Below threshold, thermal emission is expected for polaritons occupying a broad range of states in momentum space, represented by $g^{(2)}(0) = 2$. To resolve such a feature in photon statistics, high temporal-resolution is required. With a standard Hanbury-Brown and Twiss (HBT) setup[38] based on Si avalanche photo detectors, the temporal resolution (here 40 ps) of the single photon counting modules (SPCMs) is usually lower than the relevant coherence time of the emitters. Thus thermal bunching effects can only be resolved close to the quantum degeneracy threshold, when the coherence time of the emitter increases significantly.[39–41]

Standard HBT techniques were often used to identify lasing operation for various photonic microstructure systems. However, first studies of polariton condensates' second-order autocorrelation for GaAs[2] and CdTe[12] structures bore different results. While the CdTe polaritons seemingly reached a very high coherence degree at the condensation threshold, the GaAs polaritons revealed strong intensity fluctuations above the threshold at comparable pumping schemes. In the GaAs system, strong intensity fluctuations in the condensate regime were also shown by Horikiri *et al.* by an HBT second- and third-order autocorrelation experiment.[15] In parallel, Assmann *et al.* performed a power-dependent analysis of the polaritons' second- and third-order autocorrelation for different detunings and excitation schemes with a streak camera technique providing a picosecond time resolution,[14] revealing a clear dependency on the exciton-cavity detuning and the excitation polarization. Here, we reveal that the investigated autocorrelation function for a fs-pumped system in momentum-space resolved spectroscopy, i.e., measurements with strong energy-momentum resolution, shows super-Poissonian photon statistics of the emitted light well above threshold.

With a fiber-coupled HBT setup (temporal resolution: 40 ps), we record the photon autocorrelation of the ground-state emission after spectrally resolving the signal with a monochromator ($\Delta E_{\mathrm{mono}} \approx 50\,\mu$eV). Figure 6(a) presents a time-averaged second-order time correlation $G^{(2)}(\tau)$ acquisition in the Fourier-space configuration. To the right of the representative FF spectrum, the corresponding NF image is displayed in which the contributing signal is collected over with a spatial selection of ≈20 μm (images are taken from Figs. 1 and 2). The fiber's front facet with 65-μm-core diameter is placed directly in the back-focal plane of the monochromator at its lateral exit port where it acts as an aperture and allows essentially for monomode detection as required to probe the

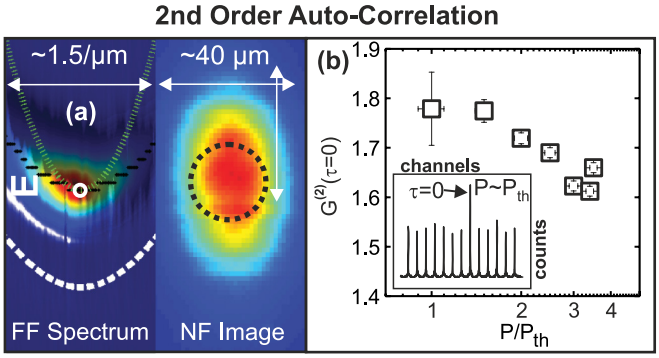

FIG. 6. (Color online) (a) Presentation of the time-averaged second-order time correlation $G^{(2)}(\tau)$ acquisition in the Fourier-space configuration with representative FF spectrum and corresponding NF image with spatial selection of $\approx 20\ \mu$m. The white circle indicates the fiber aperture, which acts as an E-k filter for light analyzed by a fiber-coupled HBT. (b) Pump-power-dependent autocorrelation function $G^{(2)}(\tau = 0)$ measured with an HBT setup for the pulsed polariton ground-state emission in the FF projection. (Inset) Representative correlation histogram.

photon coalescence from the condensate. The obtained filtering is $\approx 150\ \mu$eV and $\approx 0.02\ \mu\text{m}^{-1}$ in E-k for FF, as indicated schematically in Fig. 6(a). Thus the results presented in Fig. 6 were obtained under well-defined experimental conditions by adjusting for maximum intensity for each pump power.

We show in the following that there exist quantitative differences in the detected $G^{(2)}(0)$ values of the condensate emission compared with photon statistics of an ideal coherent state characterized by $G^{(2)}(0) = 1$. In the ground-state emission sensitive FF $G^{(2)}$ experiment, which selects a specific region close to $k_{||} = 0$ in the energy-momentum dispersion, a high bunching value is observed for polariton condensates around the threshold even with a time-resolution limited HBT setup: since the ground-state's photonic content is higher and decay-rates are higher than for the much more excitonic reservoir states, here about half of the cavity decay rate at this detuning, the signal pulse width becomes comparable to the coherence time for the condensate due to stimulated scattering into the ground state.[2] Thus $G^{(2)}(0)$ (time-averaged function) well represents $g^{(2)}(0)$.

The $G^{(2)}$ data in Fig. 6(b) could only be efficiently acquired above threshold, because of a very weak ground-state population below threshold, where $G^{(2)}(0) = 2$. To account for the fast dynamics of the polaritonic system, we used fast Si-SPCMs with a temporal resolution of 40 ps, which can only be obtained at the cost of lower quantum efficiency ($\approx$5–7% at 800 nm), if compared to standard Si-SPCMs with a temporal resolution of about 1 ns and a quantum efficiency of 60% at 800 nm. Due to a setup collection efficiency of $\approx$0.1% in the FF configuration, and applied strong filtering of the polaritonic emission in the FF plane, we detected only a small fraction ($\approx 10^{-6}$) of the total emission in the HBT setup with count rates of the SPCMs amounting to 3000–4000 counts/s at the lowest excitation power measured ($P = P_{\text{th}}$) in FF configuration. From mode energy, lifetime, and polariton density of the ground state, we estimate cavity emission powers below threshold to be $\approx$1nW, corresponding to a flux of $\approx 4 \times 10^9$ photons/s, explaining the low count rates.

In our experiment, $G^{(2)}(0)$ of 1.75 was obtained at P_{th}. The inset in Fig. 6(b) presents the corresponding correlation histogram at P_{th} in a representative manner. The autocorrelation function then decreases gradually with increased power to $\approx$1.65 at 4 P_{th}, while for a fully coherent emitter a reduction to $G^{(2)}(0) = 1$ is expected. These intensity fluctuations above threshold can be interpreted as an indication of either dephasing effects due to a strong interaction between polaritons in the condensed state,[12,14,15] or of an incomplete thermalization process within the lifetime of condensed particles, while scattering processes are efficient enough to build up the macroscopic occupation of the ground state.[2,42] The $G^{(2)}$ trend is comparable to the data presented in Ref. 2 by Deng *et al.* who mapped the transition and measured a decrease of the ground state $G^{(2)}(0)$ from $\approx$1.8 at threshold to $\approx$1.5 even at 15 P_{th} for resonance detuning. This trend clearly differs from presented data for GaAs QWs in Ref. 14, where values above threshold decreased from $G^{(2)}(0) \approx 1.5$ at P_{th} (thermal bunching level for polarization-independent acquisition) and even reached 1 at ≈ 10 P_{th} for the spectrally filtered sample emission at a comparable positive detuning ($\Delta = +2$ meV) and for a similar pumping scheme. This indicates that the latter result represents a thermalized, weakly interacting system which, indeed, can reach full coherence high above threshold,[14,43] while the first describes a condensed state still out of equilibrium for even higher pump rates. Here, small statistical errors for $G^{(2)}$ values falling below the symbol sizes are shown in Fig. 6(b).

Acquired photon statistics for our polariton condensate strongly indicate that the coherence properties differ from that of a standard photon laser, because the transition from bunching to $G^{(2)} = 1$ for $P > P_{\text{th}}$ is missing. Schwendimann *et al.* attributed these intensity fluctuations corresponding to a partially coherent state as a consequence of polariton-polariton scattering in a sense that such interaction prevents the condensate to be fully accumulated (condensate fraction n_0/n is reduced) and introduces a strong noise component in its photon statistics.[44] The calculated pump-power-dependent auto-correlation for $k = 0$ polaritons taking into account interaction between ground-state polaritons with themselves as well as with high-k polaritons well matches with our experimental results.

In the FF configuration, spectral and momentum-space selection together guarantee an attractive probe of the ground-state emission in the time-integrated system when adjusted to maximum intensity on the energy scale—the condensate at the time of maximum build-up and decay—also reducing averaging effects. In this configuration, the autocorrelation signal at selected k vectors (here $k_{||} = 0$) is real-space integrated, but since stemming from one macroscopically occupied ground state (low-momentum emission is filtered out), the measured $G^{(2)}(0)$ is representative for the condensate.

However, for large condensates (e.g., 20–30 μm lateral extention) with short spatial coherence length (e.g., 4 μm) this also implies that, although occupation of one ground-state takes place over a relatively large area, the measured degree of coherence is reduced when collecting a spatially integrated signal. In other words, if condensate size and coherence length are comparable, such FF $G^{(2)}$ experiments could yield a higher coherence degree for ground-state emission above a condensation threshold. We conclude that second-order autocorrelation

clearly reveals polariton repulsive interaction throughout our nonequilibrium condensate with a spatial coherence length, which is shorter than the condensate extension of 20–30 μm.

V. CONCLUSIONS

In summary, we have presented a comprehensive power-dependent characterization of the exciton-polaritons' transition to a dynamical condensate in a GaAs QW-microcavity sample under a fs-pulsed side-pump excitation covering the most relevant features: we have shown spectral signatures, spontaneous build-up of spatial coherence and, most importantly, the second-order autocorrelation of condensate emission, serving with a compilation of useful tools for condensate characterization. By a two-spot interference experiment, we identified a spatial coherence length of up to 4 μm. Moreover, we discussed a modification of the polariton emission with a change of dispersion and blue shift above the quantum degeneracy corresponding to high pump powers. A pump-density dependent decrease of the effective polariton mass above threshold is identified with respect to this. In the last, we have demonstrated a nonequilibrium ground-state occupation within the lifetime of polaritons in the high-Q cavity, featuring a pronounced degree of intensity fluctuations above the condensation threshold. With our HBT setup, we acquired second-order correlation in the Fourier-space configuration with strong energy-momentum selectivity. Our results indicate polariton repulsive interaction throughout the condensate and a spatial coherence length being shorter than the condensate extension of 20-30 μm. We suggest that these results could be particularly useful for identification of polariton condensation in optically and electrically driven QW-microcavity samples. Moreover, they could trigger a further collection of identification tools in the field of exciton-polariton nonlinearities.

ACKNOWLEDGMENTS

The authors acknowledge financial support by the State of Bavaria and thank K. McLeod, A. Cavers, and T. Masuda for experimental and technical support.

*arash.rahimi-iman@physik.uni-wuerzburg.de

†Present address: Institut für Festkörperphysik, Technische Universität Berlin, Hardenbergstrasse 36, D-10623 Berlin, Germany.

[1] C. Weisbuch, M. Nishioka, A. Ishikawa, and Y. Arakawa, Phys. Rev. Lett. **69**, 3314 (1992).

[2] H. Deng, G. Weihs, C. Santori, J. Bloch, and Y. Yamamoto, Science **298**, 199 (2002).

[3] J. Kasprzak, M. Richard, S. Kundermann, A. Baas, P. Jeambrun, J. M. J. Keeling, F. M. Marchetti, M. H. Szymanska, R. Andre, J. L. Staehli, V. Savona, P. B. Littlewood, B. Deveaud, and L. S. Dang, Nature (London) **443**, 409 (2006).

[4] R. Balili, V. Hartwell, D. Snoke, L. Pfeiffer, and K. West, Science **316**, 1007 (2007).

[5] S. Christopoulos, G. Baldassarri Höger von Högersthal, A. Grundy, P. G. Lagoudakis, A. V. Kavokin, J. J. Baumberg, G. Christmann, R. Butté, E. Feltin, J.-F. Carlin, and N. Grandjean, Phys. Rev. Lett. **98**, 126405 (2007).

[6] L. Sun, S. Sun, H. Dong, W. Xie, M. Richard, L. Zhou, L. S. Dang, X. Shen, and Z. Chen, arXiv:1007.4686v1 (unpublished).

[7] A. Das, J. Heo, M. Jankowski, W. Guo, L. Zhang, H. Deng, and P. Bhattacharya, Phys. Rev. Lett. **107**, 066405 (2011).

[8] M. H. Anderson, J. R. Ensher, M. R. Matthews, C. E. Wieman, and E. A. Cornell, Science **269**, 198 (1995).

[9] K. B. Davis, M. O. Mewes, M. R. Andrews, N. J. van Druten, D. S. Durfee, D. M. Kurn, and W. Ketterle, Phys. Rev. Lett. **75**, 3969 (1995).

[10] C. W. Lai, N. Y. Kim, S. Utsunomiya, G. Roumpos, H. Deng, M. D. Fraser, T. Byrnes, P. Recher, N. Kumada, T. Fujisawa, and Y. Yamamoto, Nature (London) **450**, 529 (2007).

[11] H. Deng, G. S. Solomon, R. Hey, K. H. Ploog, and Y. Yamamoto, Phys. Rev. Lett. **99**, 126403 (2007).

[12] J. Kasprzak, M. Richard, A. Baas, B. Deveaud, R. Andre, J.-Ph. Poizat, and L. S. Dang, Phys. Rev. Lett. **100**, 067402 (2008).

[13] J. Kasprzak, D. D. Solnyshkov, R. André, Le Si Dang, and G. Malpuech, Phys. Rev. Lett. **101**, 146404 (2008).

[14] M. Aßmann, J.-S. Tempel, F. Veit, M. Bayer, A. Rahimi-Iman, A. Löffler, S. Höfling, S. Reitzenstein, L. Worschech, and A. Forchel, Proc. Natl. Acad. Sci. USA **108**, 1804 (2011).

[15] T. Horikiri, P. Schwendimann, A. Quattropani, S. Höfling, A. Forchel, and Y. Yamamoto, Phys. Rev. B **81**, 033307 (2010).

[16] E. Kammann, M. Maragkou, A. J. D. Grundy, A. K. Kavokin, and P. G. Lagoudakis, arXiv:1103.4831.

[17] A. V. Larionov, V. D. Kulakovskii, S. Höfling, C. Schneider, L. Worschech, and A. Forchel, Phys. Rev. Lett. **105**, 256401 (2010).

[18] P. Walker, T. C. H. Liew, D. Sarkar, M. Durska, A. P. D. Love, M. S. Skolnick, J. S. Roberts, I. A. Shelykh, A. V. Kavokin, and D. N. Krizhanovskii, Phys. Rev. Lett. **106**, 257401 (2011).

[19] G. Roumpos, C. W. Lai, T. C. H. Liew, Y. G. Rubo, A. V. Kavokin, and Y. Yamamoto, Phys. Rev. B **79**, 195310 (2009).

[20] A. A. Demenev, S. S. Gavrilov, and V. D. Kulakovski, JETP Lett. **95**, 38 (2012).

[21] B. Deveaud-Plédran, J. Opt. Soc. Am. B **29**, A138 (2012).

[22] R. Houdré, J. L. Gibernon, P. Pellandini, R. P. Stanley, U. Oesterle, C. Weisbuch, J. O'Gorman, B. Roycroft, and M. Ilegems, Phys. Rev. B **52**, 7810 (1995).

[23] J. Bloch, B. Sermage, M. Perrin, P. Senellart, R. André, and Le Si Dang, Phys. Rev. B **71**, 155311 (2005).

[24] The optical quality (Q) factor of the microresonator given in this paper was determined by preparing micropillars with a diameter of 4 μm from a red detuned region of the wafer with a low excitonic content of <10% (detuning $\Delta = E_C - E_X \approx -10$ meV, where E_C denotes the spectral position of the cavity mode and E_X the exciton ground-state energy). Determining the Q factor by this method is more reliable if compared to simple reflection experiments performed on planar samples because it facilitates the measurement of Q for $k \to 0$.

[25] H. Deng, G. Weihs, D. Snoke, J. Bloch, and Y. Yamamoto, Proc. Natl. Acad. Sci. USA **100**, 15318 (2003).

[26] D. Bajoni, P. Senellart, A. Lemaître, and J. Bloch, Phys. Rev. B **76**, 201305(R) (2007).

[27]G. Roumpos, W. H. Nitsche, S. Höfling, A. Forchel, and Y. Yamamoto, Phys. Rev. Lett. **104**, 126403 (2010).

[28]S. Utsunomiya, L. Tian, G. Roumpos, C. W. Lai, N. Kumada, T. Fujisawa, M. Kuwata-Gonokami, A. Löffler, S. Höfling, A. Forchel, and Y. Yamamoto, Nat. Phys. **4**, 700 (2008).

[29]With the described technique of spatial coherence measurement, the coherently emitting mode can be easily determined in the FF spectrum at one glance, because the fringes that occur above threshold are specifically attributed to this mode, a feature not available in the simple FF projection plane. In case of multiple coherent modes, each spectrally resolved coherent mode can be individually analyzed without any super-position of interference patterns. This gives unique options to spectroscopy of simultaneously occurring lasing regimes, e.g., spectrally separated photon lasing and polariton condensation in a time-integrated acquisition, or competing lasing modes in multimode emitters.

[30]For the applied optical configuration, both k-space (k_x-k_y) or spectral resolution (k_x-E) can be achieved.

[31]H. Deng, H. Haug, and Y. Yamamoto, Rev. Mod. Phys. **82**, 1489 (2010).

[32]C. Ciuti, V. Savona, C. Piermarocchi, A. Quattropani, and P. Schwendimann, Phys. Rev. B **58**, 7926 (1998).

[33]G. Rochat, C. Ciuti, V. Savona, C. Piermarocchi, A. Quattropani, and P. Schwendimann, Phys. Rev. B **61**, 13856 (2000).

[34]S. Schmitt-Rink, D. S. Chemla, and D. A. B. Miller, Phys. Rev. B **32**, 6601 (1985).

[35]T. D. Doan, H. T. Cao, D. B. Tran Thoai, and H. Haug, Phys. Rev. B **78**, 205306 (2008).

[36]T. D. Doan, H. Thien Cao, D. B. Tran Thoai, and H. Haug, Solid State Commun. **145**, 48 (2008).

[37]H. Deng, D. Press, S. Gotzinger, G. S. Solomon, R. Hey, K. H. Ploog, and Y. Yamamoto, Phys. Rev. Lett. **97**, 146402 (2006).

[38]R. Hanbury Brown and R. Twiss, Nature (London) **177**, 27 (1956).

[39]Bunching can be resolved if the coherence time is close to the temporal resolution of the HBT setup or becomes comparable to the pulse duration. Above threshold, the expected transition to $g^{(2)}(0) = 1$ for a coherent emitter can be observed due to an increased coherence time with increasing power, which results in a characteristic bunching behavior with a peak in $g^{(2)}(0)$ around P_{th}.

[40]S. Strauf, K. Hennessy, M. T. Rakher, Y.-S. Choi, A. Badolato, L. C. Andreani, E. L. Hu, P. M. Petroff, and D. Bouwmeester, Phys. Rev. Lett. **96**, 127404 (2006).

[41]S. M. Ulrich, C. Gies, S. Ates, J. Wiersig, S. Reitzenstein, C. Hofmann, A. Löffler, A. Forchel, F. Jahnke, and P. Michler, Phys. Rev. Lett. **98**, 043906 (2007).

[42]N. G. Vy, H. T. Cao, D. B. Tran Thoai, and H. Haug, Phys. Rev. B **80**, 195306 (2009).

[43]J.-S. Tempel, F. Veit, M. Assmann, L. E. Kreilkamp, A. Rahimi-Iman, A. Löffler, S. Höfling, S. Reitzenstein, L. Worschech, A. Forchel, and M. Bayer, Phys. Rev. B **85**, 075318 (2012).

[44]P. Schwendimann and A. Quattropani, Phys. Rev. **77**, 085317 (2008).